Extreme Localization of Fields in Open Cylindrical Impedance Surface Cavities

Jacobsen, Rasmus E.; Arslanagic, Samel

Published in:
IEEE Transactions on Antennas and Propagation

Link to article, DOI:
10.1109/TAP.2024.3349783

Publication date:
2024

Document Version
Peer reviewed version

Extreme Localization of Fields in Open Cylindrical Impedance Surface Cavities

Rasmus E. Jacobsen, and Samel Arslanagić, *Senior Member, IEEE*

***Abstract*—Bound states in the continuum as well as their approximations are highly localized modes enabling extreme wave-matter interactions. While typically found in array-type of structures, recent efforts have demonstrated versions of such states in cavity slabs formed by surface impedance sheets. However, such slab configurations are not suitable for free-space excitations due to large sizes of the underlying impedance surfaces. To alleviate these issues, the present work introduces an open cavity made of a single cylindrical impedance surface for extreme field localizations. The overall structure behaves as a quasi-open cavity, enabled by overlapping resonances in the cavity and the impedance surfaces, effectively forming a quasi bound state in the continuum. A cavity formed of conductive strips of Jerusalem crosses is designed in the microwave part of the spectrum and analyzed by analytical and numerical means. The analytical solution, which assumes a homogeneous impedance surface, predicts a quality factor of ~$7 \cdot 10^{10}$, whereas the numerical quality factor is 3,000 due to material losses and inhomogeneity of the modelled impedance surface fully accounted for in the numerical model. The proposed resonator may find applications within filters, antennas, sensing and nonlinear devices.**

***Index Terms*—Bound states in the continuum, Embedded eigenstates, Cavity resonators**

I. Introduction

THE ability to confine fields is of vital importance in a wide variety of electromagnetic systems. The typical device is a partially open or fully closed cavity driven in a resonant state with minimal energy leakage and absorption. For example, at microwave frequencies, metallic walls are used to form fully closed cavities enabling modes with very high quality factors (Q-factors), but such configurations cannot be excited by external waves. On the other hand, optical Fabry-Pérot interferometers are open structures, which consist of two partially open/closed mirrors. They exploit interference of waves to concentrate the field within the mirrors, but they typically suffer from phase-lagging and low overall efficiency.

Lately, there has been an immense focus on wave-trapping in open structures [1]–[4]. Such structures utilize highly resonant states, which lie inside the continuum, but remain localized with no radiation. These states, also known as bound states in the continuum (BICs), are typically found in photonic (periodic) configurations as well as structures with extreme material parameters, such as epsilon-near-zero materials [5], [6]. BICs are typically classified by the number of eigenmodes involved as well as the underlying interference mechanism, which is either related to the symmetry of the structure (symmetry-protected BICs) or the Friedrich-Wintgen mechanism (accidental BICs). Theoretically, BICs have infinite Q-factors, but due to structural disorders and/or material absorptions, the Q-factor is finite. Moreover, reasonable coupling must be enabled for practical usage of the resonant states, which is achieved by slightly detuning the system away from the BIC. The excited states are often referred to as quasi-BICs. For non-periodic structures, the maximum local field scales with the Q-factor of the underlying resonant system. The BICs in arrays are extended in space, and therefore they do not support large local density of states [5]. On the contrary, BICs in single dielectric and metallic resonators show great field localizations [7]–[10].

Recently, quasi-BICs were demonstrated in a cavity consisting of a slab of two metasurfaces or impedance surfaces (ISs) [11]. ISs are surface structures with effective surface impedances $Z_{\mathrm{S}} = R_{\mathrm{S}} + jX_{\mathrm{S}}$, where R_{S} and X_{S} are the corresponding resistance and reactance, respectively. Quasi-BICs occur when the ISs of the slab are identical or complimentary, i.e. $Z_{\mathrm{S1}} = \pm Z_{\mathrm{S2}}$, and the distance between the ISs is $n\lambda/2$, with λ and n being the wavelength and an integer number, respectively. For passive ISs, $R_{\mathrm{S}} \geq 0$ and the resonance condition is then $X_{\mathrm{S1}} = \pm X_{\mathrm{S2}}$. A BIC emerges when the ISs are perfect electric conductors (PECs), i.e. $Z_{\mathrm{S1}} = Z_{\mathrm{S1}} = 0$, making the cavity fully closed for any external excitation. However, for small, but none-zero, surface impedances, a quasi-BIC can be excited with a very high Q-factor. A Q-factor of 414 was demonstrated experimentally at microwave frequencies using non-resonant ISs with surface reactances $\pm 31\ \Omega$, which were placed in a metallic waveguide setup. To further increase the Q-factor, the surface impedances must be reduced, and thus resonant ISs are needed. However, the configuration holds general limitations such as the IS size required for efficient excitation using free-space waves as well as the sensitivity to changes in the incident angle.

The purpose of this work is to investigate quasi-BIC resonators consisting of cylindrical IS cavities, see Fig. 1(a). Cylindrical ISs have been used in various applications, including cloaking and antenna devices [12]–[15] as well as in superscattering structures breaking the fundamental single-

Manuscript received Month Date, Year; revised Month Date, Year; accepted Month Date, Year. Date of publication Month Date, Year; date of current version Month Date, Year. *(Corresponding author: R. E. Jacobsen).*

Rasmus E. Jacobsen and Samel Arslangić are with the Department of Space Research and Technology, Technical University of Denmark, Bld. 348, Ørsteds Plads, 2800 Kgs. Lyngby, Denmark (e-mail: rajac@dtu.dk, saar@dtu.dk)

Color versions of one or more of the figures in this article are available online at http://ieeexplore.ieee.org

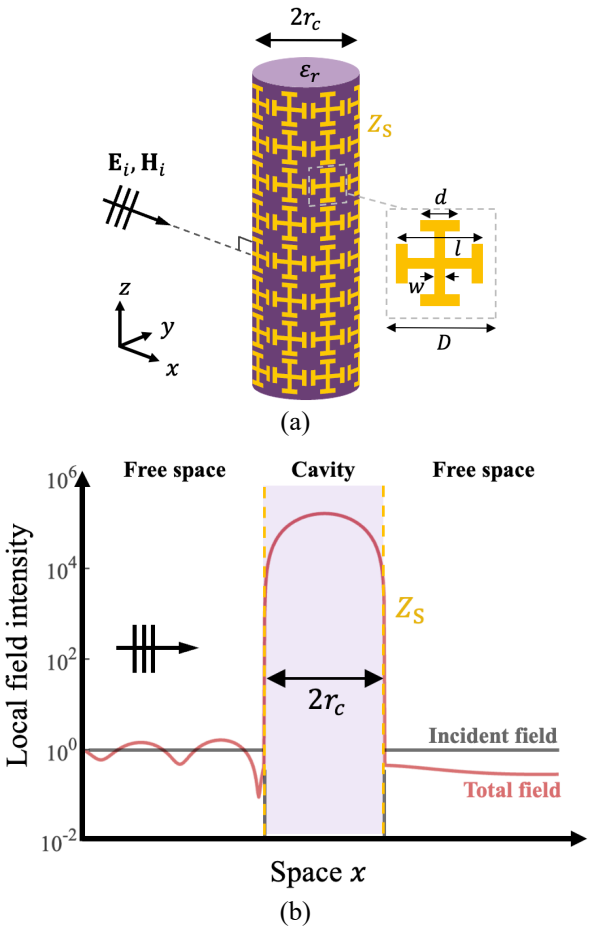

Fig. 1. Extreme field localization enabled by quasi-BICs formed in a cylindrical impedance surface cavity. (a) Sketch of the configuration and (b) the intensity of the local z-directed field for a quasi-BIC mode ($n = 0$).

channel limit [16], which have been of great interest in recent time [17], [18]. Recently, it was also demonstrated that cylindrical ISs can be designed with enhanced as well as suppressed scattering responses [19]. However, there has been limited attention towards the quasi-BIC case, where Z_S is close to zero, and this has primarily concerned the use in circular waveguides [20], [21]. The present work comprises both the theoretical and numerical basis of cylindrical IS cavities, which may find applications within filters, antennas, sensing and nonlinear devices. We demonstrate the existence of BICs in cylindrical ISs, which emerge when the natural resonances of the IS cavity coincide with the resonance of the IS effectively forming a closed cavity. The interference mechanism of the observed BICs is related to the symmetry of the structure, and they are therefore classified as single-mode symmetry-protected BICs. In the case when Z_S is a small, but non-zero value, a quasi-BIC can be excited by an external wave resulting in an extreme field concentration inside the IS cavity, but with minimal changes to the scattering outside, see Fig. 1(b). In the case of $Z_S = 0$, the IS cavity is closed and cannot be excited by any external waves. The canonical configuration permits an analytical approach, and its solution is presented and used to determine the resonant properties of the IS cavity in Section II. In Section III, the resonant properties of IS cavities are studied. First, the local field enhancement and the scattering efficiency are investigated for different cavity sizes and surface impedances. Second, the first three modes are studied by their local field distribution as well as how their Q-factor and resonance sizes are affected by dielectric loading and the surface reactance and resistance (losses) of the IS. A realistic IS made of conductive strips of Jerusalem crosses is investigated analytically and numerically in Section IV. The final configuration includes both the dispersion, inhomogeneity and material losses of the IS showing a Q-factor of around 3,000. At last, Section V summarizes the various presented cases and their associated details. Throughout the work, the time factor $\exp(j\omega t)$, where ω is the angular frequency and t is the time, have been assumed and suppressed.

II. Analytical Expressions and Resonance Conditions

A. The Configuration and Field Coefficients

The configuration under study is an infinitely long circular cylindrical cavity of radius r_c consisting of a surface impedance Z_S surrounding a dielectric medium with the relative permittivity ε_r, see Fig. 1(a). A rectangular coordinate system (x, y, z) is placed with the z-axis coincident with the cylinder axis, and the IS cavity is illuminated by a linearly polarized plane wave propagating in the $+x$-direction. The analytical solutions to the scattered and internal field coefficients have been derived using the impedance boundary conditions [22], as well as the classical Lorentz–Mie analysis for cylindrical harmonics [23]. The final expressions for the scattered field coefficients are given in Eqs. (1) and (2) for the transverse magnetic (TM) and transverse electric (TE) incidences, respectively. The internal field coefficients are given by

$$b_n^{\mathrm{TM}} = \frac{J_n(x_0) + a_n^{\mathrm{TM}} H_n^{(2)}(x_0)}{J_n(mx_0)} \tag{3}$$

and

$$a_n^{\mathrm{TM}} = \frac{J_n'(x_0)J_n(mx_0) - mJ_n(x_0)J_n'(mx_0) + \frac{1}{jZ_{S0}}J_n(x_0)J_n(mx_0)}{mH_n^{(2)}(x_0)J_n'(mx_0) - H_n^{(2)\prime}(x_0)J_n(mx_0) - \frac{1}{jZ_{S0}}H_n^{(2)}(x_0)J_n(mx_0)} \tag{1}$$

$$a_n^{\mathrm{TE}} = \frac{J_n(x_0)J_n'(mx_0) - mJ_n'(x_0)J_n(mx_0) - \frac{1}{jZ_{S0}}J_n'(x_0)J_n'(mx_0)}{mH_n^{(2)\prime}(x_0)J_n(mx_0) - H_n^{(2)}(x_0)J_n'(mx_0) + \frac{1}{jZ_{S0}}H_n^{(2)\prime}(x_0)J_n'(mx_0)} \tag{2}$$

$$b_n^{\mathrm{TE}} = \frac{J_n'(x_0) + a_n^{\mathrm{TE}} H_n^{(2)\prime}(x_0)}{J_n'(mx_0)}, \tag{4}$$

where $m = \sqrt{\varepsilon_r}$, $Z_{\mathrm{S0}} = Z_{\mathrm{S}}/\eta_0$ and $x_0 = 2\pi r_{\mathrm{c}}/\lambda_0$ with λ_0 and η_0 being the wavelength and intrinsic impedance in free space, respectively. Moreover, $J_n(\cdot)$ is the nth order Bessel function of the first kind and $H_n^{(2)}(\cdot)$ is the nth order Hankel function of the second kind. The prime $'$ denotes the derivative with respect to the entire argument.

B. Resonance Conditions

For low-loss surface impedances with very small (but non-zero) surface reactances, i.e. $X_{\mathrm{S}} \ll \eta_0/m$, the scattering coefficients in Eqs. (1) and (2) can be approximated as $a_n^{\mathrm{TM}} \approx \Delta_{\mathrm{TM}} - J_n(x_0)/H_n^{(2)}(x_0)$ and $a_n^{\mathrm{TE}} \approx \Delta_{\mathrm{TE}} - J_n'(x_0)/H_n^{(2)\prime}(x_0)$, respectively, where Δ_{TM} and Δ_{TE} are small constants. Substituting these into Eqs. (3) and (4), the internal field coefficients of the resonant IS cavity are approximated as

$$b_n^{\mathrm{TM}} \approx \frac{\Delta_{\mathrm{TM}} H_n^{(2)}(x_0)}{J_n(mx_0)} \approx \frac{\delta_{\mathrm{TM}}}{J_n(mx_0)}$$
$$b_n^{\mathrm{TE}} \approx \frac{\Delta_{\mathrm{TE}} H_n^{(2)\prime}(x_0)}{J_n'(mx_0)} \approx \frac{\delta_{\mathrm{TE}}}{J_n'(mx_0)} \tag{5}$$

where δ_{TM} and δ_{TE} are small constants. If $X_{\mathrm{S}} = 0$ (PEC case), then $\Delta_{\mathrm{TM}} = \Delta_{\mathrm{TE}} = \delta_{\mathrm{TM}} = \delta_{\mathrm{TE}} = 0$ such that $b_n^{\mathrm{TM}} = b_n^{\mathrm{TE}} = 0$, and we obtain the well-known scattering coefficients for a PEC cylinder, $a_n^{\mathrm{TM}} = -J_n(x_0)/H_n^{(2)}(x_0)$ and $a_n^{\mathrm{TE}} = -J_n'(x_0)/H_n^{(2)\prime}(x_0)$ [22].

From Eq. (5), it is found that the resonance conditions are the zeroes of $J_n(mx_0)$ and $J_n'(mx_0)$ for the TM and TE polarizations, respectively. This is illustrated in Fig. 2, which shows the magnitudes of the internal field coefficients (Eq. (3), (4)) and the reciprocal Bessel functions in Eq. (5) as functions of mx_0 for an empty ($m = 1$) and lossless ($R_S = 0$) IS cavity with $Z_{\mathrm{S0}} = j0.001$. Significant peaks are observed in the internal field coefficients for various modes (n). Furthermore, these peaks coincide with the resonance conditions found for the approximated coefficients in Eq. (5).

Even though the present configuration is open, and thus different from closed cylindrical cavities and circular waveguides, their resonance conditions are very similar [22]. In fact, when $Z_{\mathrm{S0}} = 0$, i.e. a PEC surface, the cavity is closed and the fields inside the cavity are zero ($b_n^{\mathrm{TM}} = b_n^{\mathrm{TE}} = 0$). The incident field cannot penetrate the PEC surface, and thus no resonances are excited. For very small Z_{S0}, the IS cavity is partially open and thus supports resonances with high Q-factors, which can be excited by external waves. From Fig. 2, it is noted that the smallest resonance size is different for the two polarizations, namely $mx_0 \approx 2.4$ ($mx_0 \approx 1.8$) for the TM (TE) incidence. Moreover, the $n = 1$ mode of the TM incidence has the same resonance size ($mx_0 \approx 3.8$) as the $n = 0$ mode of the TE incidence.

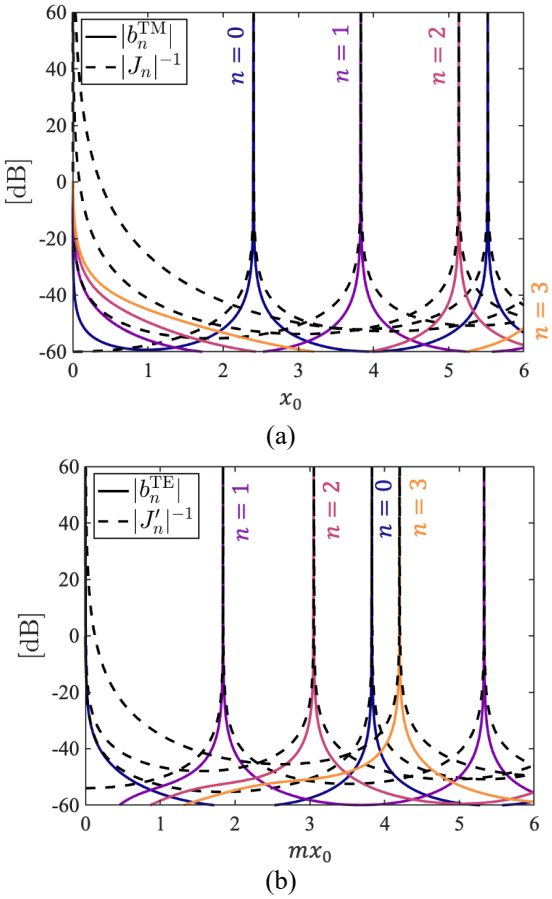

Fig. 2. Resonances for the modes in the empty and lossless IS cavity. The figures show the reciprocal of the Bessel functions and the internal field coefficients as functions of the size parameter mx_0 for a cavity with $m = 1$ and $Z_{\mathrm{S0}} = j0.001$. The polarization is TM in (a) and TE in (b).

III. Cavity With Non-Dispersive and Homogeneous IS

A. Resonances in the Empty IS Cavity

As the IS cavity is open, both the local and scattered fields are investigated. The scattering efficiency is used to evaluate the total scattering from the IS cavity and is determined as $Q_{\mathrm{sca}}^P = (2/x_0)\sum_{n=-\infty}^{\infty}|a_n^P|^2$ with P denoting the polarization (TM or TE). The Q_{sca}^P and the respective local z-directed field intensities are shown as functions of x_0 in Fig. 3 for empty IS cavities with different lossless surface impedances Z_{S0}. The local fields are evaluated at coordinates $(x, y) = (r_{\mathrm{c}}/2, 0)$. For IS cavities with small Z_{S0}, the change in Q_{sca}^P around the resonances is very small for both polarizations compared to the increase in the local field intensity inside the IS cavity. This peculiar behavior is very different than other open resonators such as split-ring resonators and dielectric resonators, which typically exhibit large increases in their scattered fields around resonances. Interestingly, the scattering response of the IS cavity becomes similar to that of dielectric resonators, when the surface impedance is comparable with the intrinsic impedance of the surrounding space. In this case, the sign of Z_{S0} also becomes important and has a great impact on the scattering response, see e.g. [14], [24] for more information.

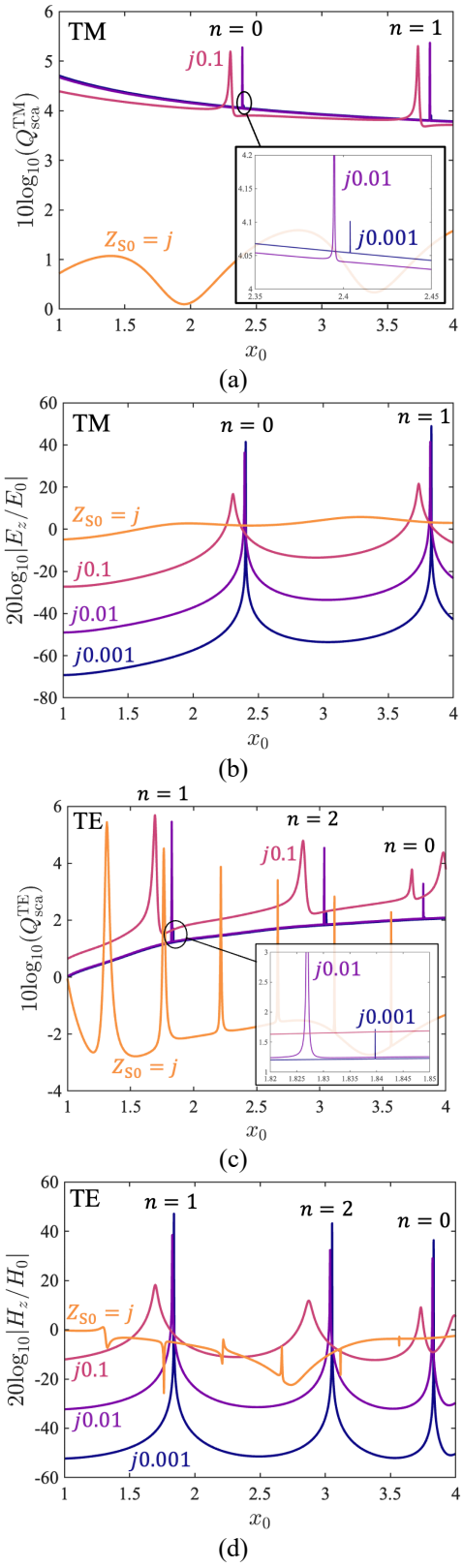

Fig. 3. Total scattering and local field intensity of empty and lossless IS cavities. (a) and (c) show the scattering efficiency (Q_{sca}^{P}), and (b) and (d) the intensity of the local z-directed field, as functions of x_0 for different surface impedances Z_{S0}. All y-axes are shown in logarithmic scale. (a) and (b) [(c) and (d)] show the results for the TM [TE] incidence. Insets are included in (a) and (c) to show the low-scattering resonance for the case $Z_{\mathrm{S0}} = j0.001$. The local fields are evaluated at coordinates $(x, y) = (r_{\mathrm{c}}/2, 0)$ and E_0 (H_0) is the incident electric (magnetic) field magnitude.

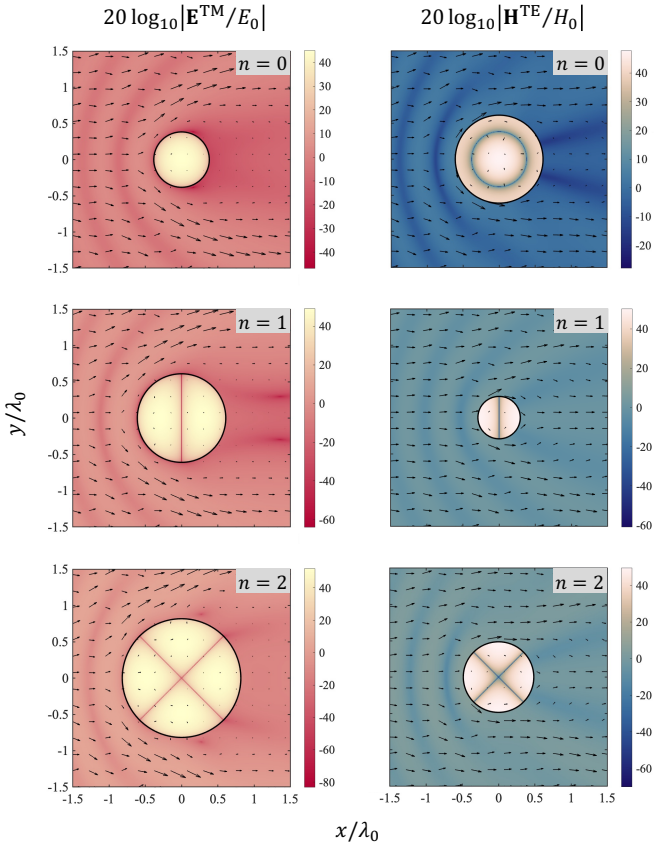

Fig. 4. The local field magnitude (colors) and power flow density (arrows) in the xy-plane of different empty and lossless IS cavities ($Z_{\mathrm{S0}} = j0.001$, $m = 1$) at their resonance sizes. Left (right) panel shows the electric (magnetic) field for the TM (TE) polarization for cavity sizes $x_0^{n=0} = 2.40382$, $x_0^{n=1} = 3.83071$ and $x_0^{n=2} = 5.13462$ ($x_0^{n=0} = 3.83071$, $x_0^{n=1} = 1.83976$ and $x_0^{n=2} = 3.05248$). The incident plane wave propagates in the $+x$-direction. The scale of the colors and arrows is logarithmic.

The local z-directed field (colors) is shown in the xy-plane in Fig. 4 for resonant IS cavities with $Z_{\mathrm{S0}} = j0.001$. The results for the resonant modes $n = 0, 1$ and 2 for both TM and TE incidences are included. The field is clearly enhanced inside the IS cavity, due to the excited resonances, whereas the outside scattered field is similar to that of a PEC cylinder. The power flow density is included in Fig. 4 (shown as arrows), and there is a distinct power flow around the IS cavity and minimal power flow inside. This is expected as there are mainly standing waves inside the cavity. The maximum field is approximately 300 times larger than the incident field for all resonant IS cavities, and is limited by the localization properties of the IS, i.e., the non-zero value of Z_{S0}. Reducing Z_{S0} even further increases the maximum field and the Q-factor until $Z_{\mathrm{S0}} = 0$, where the fields inside the IS cavity vanishes.

B. Q-Factor, Losses and Dielectric Loading

The Q-factors of the modes n = 0, 1 and 2 as functions of $\mathrm{Im}\{Z_{\mathrm{S0}}\} = X_{\mathrm{S0}}$ are shown in Fig. 5(a) for the lossless configuration. The results for both the TM (solid lines) and TE (dashed lines) polarizations are shown. The Q-factor has been calculated as $x_{0\mathrm{r}}^{n}/\Delta x_{0\mathrm{r}}^{n}$, where $x_{0\mathrm{r}}$ is the resonance size of the maximum local field and $\Delta x_{0\mathrm{r}}$ is the full width of the half

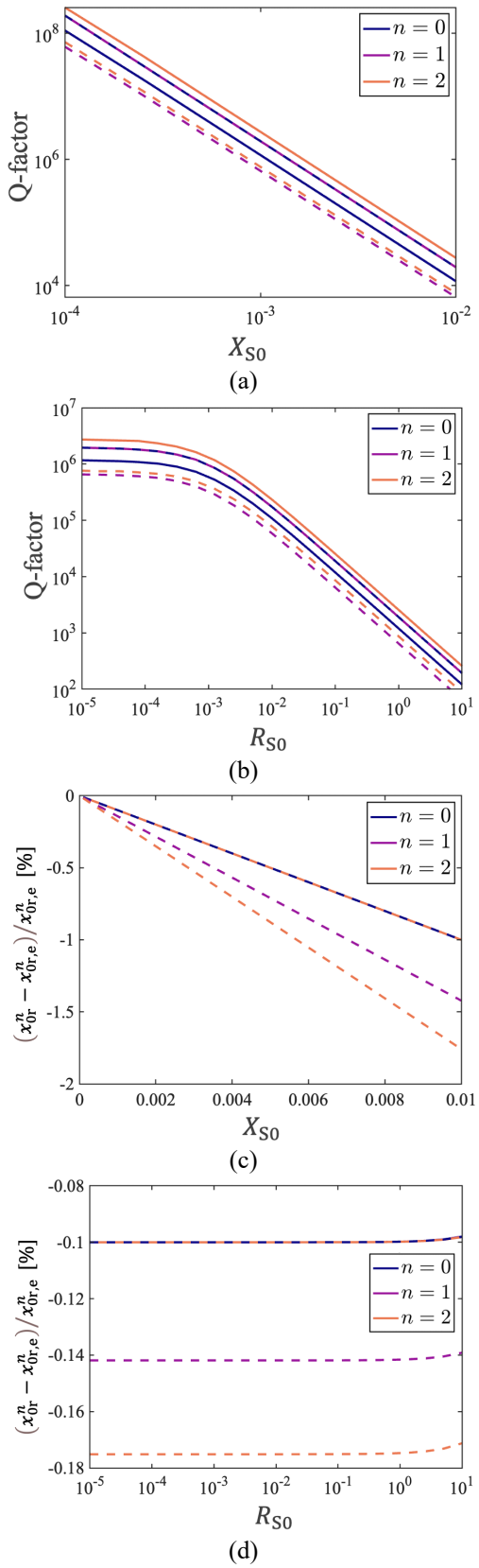

Fig. 5. The Q-factors of the modes n = 0, 1 and 2 as functions of the normalized surface reactance X_{S0} (a) and resistance R_{S0} (b) of the empty IS cavity. (c) and (d) show the relative deviations (shown as percentages) from the expected resonance sizes. The solid (dashed) lines show the results for the TM (TE) polarization. In (a) and (c), $R_{S0} = 0$, whereas $X_{S0} = 0.001$ in (b) and (d). All scales in (a) and (b), as well as the x-axis in (d), are logarithmic.

maximum. For $X_{S0} \ll 1$, the Q-factors of the modes scale with approximately $|X_S|^{-2}$. Similar results were reported in Ref. [11] for a slab of ISs. Please note that the Q-factors, as well as the resonant sizes, of modes n = 1 and n = 0 for the TM and TE polarizations, respectively, are the same. For $X_{S0} = 0.001$, the Q-factor of the modes are approximately 10^6, which will of course be affected by inevitable material losses in the IS. To investigate the effect of the losses, the Q-factor of the modes n = 0, 1 and 2 are shown in Fig. 5(b) as functions of $\mathrm{Re}\{Z_{S0}\} = R_{S0}$ for $X_{S0} = 0.001$. The Q-factors of the modes are nearly constant when $R_{S0} < |X_{S0}|$, whereas for $R_{S0} > |X_{S0}|$ they scale with ${R_{S0}}^{-1}$. This dependence on the losses in the IS is similar to closed and empty cylindrical cavities [22].

The expected resonance sizes ($x_{0r,e}^n$) are the zeroes of the Bessel functions in Eq. (5), but this is for $Z_{S0} \approx 0$, and any small variations from this criterion will cause small shifts to the resonance size. To display this dependence, we define a relative deviation as $\left(x_{0r}^n - x_{0r,e}^n\right)/x_{0r,e}^n$, which is shown as a function of X_{S0} and R_{S0} in Fig. 5(c) and (d), respectively. It is observed that changes in the surface reactance cause much greater shifts in x_{0r}^n compared to any changes to the surface resistance. Interestingly, the modes n = 1 and n = 2 of the TE incidence are more susceptible to changes in X_{S0}, whereas the modes of the TM incidence exhibit the same shift.

Thus far we have mainly considered empty cavities. In Fig. 6, the influence of loading the cavity with a dielectric is studied. The Q-factors of the modes n = 0, 1 and 2 as functions of the refractive index m of the medium inside the IS cavity with $X_{S0} = 0.001$ are shown in Fig. 6(a). The corresponding relative deviations to the expected resonance sizes are shown in Fig. 6(b). Interestingly, the tendency of the Q-factors of the modes are quite different. For media with small refractive indices (m < 2), the Q-factor is directly proportional to m for all modes, whereas for larger refractive indices (m > 2), this depends on the mode and polarization. The modes n = 1 and n = 2 of the TE incidence exhibit a significant increase in the Q-factor for larger m, indicating that the fields become more confined due to the dielectric.

In a closed and lossless cavity ($Z_{S0} = 0$), the tendency of the resonance size shift is directly proportional to m [22]. This is not entirely the case in Fig. 6(b), where small changes to the expected resonance sizes are observed. As in Fig. 5, smaller resonance sizes than the expected ones are observed. Similarly, the modes n = 1 and n = 2 of the TE incidence are also more susceptible to changes to the IS cavity.

IV. IS Cavity Realized with Jerusalem Crosses

A. Analytical Model for the Cylindrical IS Consisting of Jerusalem Crosses

Thus far we have considered non-dispersive ISs, but in practice, they will be dispersive (and hence lossy) as well as inhomogeneous. There are different ways to realize these surfaces and the choice of design and materials depends on the operating frequency [15], [19], [25]–[27]. In this work, we investigate a surface consisting of periodic elements with

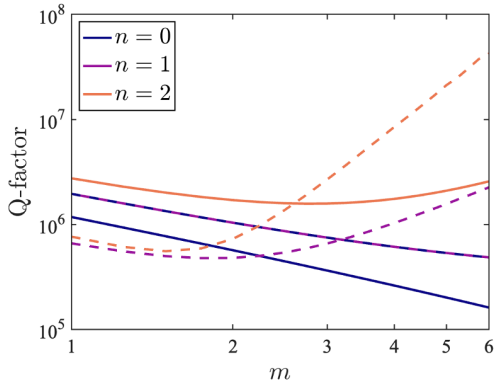

(a)

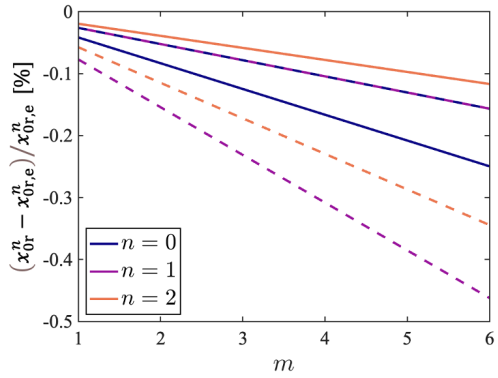

(b)

Fig. 6. (a) The Q-factors of the modes n = 0, 1 and 2 as functions of the refractive index m of the medium inside the IS cavity with $X_{S0} = 0.001$. (b) The corresponding relative deviation of the resonance size shown as a percentage. The solid (dashed) lines show the results for the TM (TE) polarization. The scales in (a) are logarithmic.

conductive strips for operation in the microwave frequency range. To realize near-zero surface impedances, resonant surfaces are required. Presently, we employ Jerusalem crosses, which provide a more compact element compared to regular crosses. A sketch of the configuration and the periodic element is shown in Fig. 1(a). The impedance of a flat impedance surface of Jerusalem crosses can be modelled as a grid of conductive strips with inductance L_g and capacitance C_g [26], such that

$$Z_S = j\omega L_g + \frac{1}{j\omega C_g} \tag{6}$$

where, for normal incidence,

$$C_g = \frac{2}{\pi}\varepsilon_r\varepsilon_0 d\left[\ln\csc\left(\frac{\pi g}{2D}\right) + F\right] \tag{7}$$

and

$$L_g = \frac{\mu_0 D}{2\pi}\ln\csc\left(\frac{\pi w}{2D}\right) \tag{8}$$

with

$$F = \frac{qu^2}{1+q(1-u)^2} + \varepsilon_{eff}\left[\frac{du(3u-2)}{4\lambda_0}\right]^2, \tag{9}$$

$$q = \sqrt{1-\varepsilon_{eff}\left(\frac{d}{\lambda_0}\right)^2},$$

$u = \cos^2(\pi g/2d)$ and μ_0 and ε_0 being the free-space permeability and permittivity, respectively. The parameter g is the width of the slit between the adjacent crosses and is thus $g = D - l$. The Jerusalem crosses have the dielectric on one side and free space on the other side, and therefore an effective permittivity, approximated as $\varepsilon_{eff} = (\varepsilon_r + 1)/2$, is employed. In our configuration, the curvature is not flat, but previous studies have shown that the above model, as well as models for other ISs, still hold with a good degree of accuracy for circular curvatures [15], [19]. Because of the circular form, the period is restricted to $D = 2\pi r_c/N$ with N being the number of elements around the circular curvature of the cylinder. The more elements one places around the cylinder, the more homogeneous the realized IS becomes, and thus the closer its effective Z_S comes to the analytical one in Eq. (6) [15], [19]. However, small deviations are expected, and therefore, full-wave simulations are required for fine-tuning of the full 3-D structure. Alternatively, full-wave simulations can also be used to retrieve the surface impedance of the real elements from the outset, see e.g., [28].

B. Cavity with Dispersive and Homogenous IS

Since the realistic surface impedance is dispersive, cf. Eqs. (6)-(9), great care must be exercised to make its resonance coincide in frequency with the one of the IS cavity. As an example, we choose the $n = 0$ mode of an empty cavity with TM incidence, see the field profile in Fig. 4 (upper left corner). The resonant size is $x_0 \approx 2.4048$ for the empty and closed cavity ($Z_{S0} = 0$), and thus $r_c \approx 0.383\lambda_{0r}$, where λ_{0r} is the resonance wavelength. We design a purely metallic IS to be resonant around the cavity resonance and the final parameters for the theoretical IS are $N = 6$, $w = 0.0408D$ and $d = 0.4D$. The surface impedance Z_{S0} is shown as a function of x_0 in Fig. 7(a) for three different values of l/D, where all graphs cross $Z_{S0} = 0$. The model of the IS is implemented into the analytical calculations and the spectrum of the electric field intensity at $(x, y) = (0,0)$ is shown in Fig. 6(b). It is observed that $l/D = 0.805$ provides the maximum field enhancement (~100 dB) and largest Q-factor (~$7\cdot10^{10}$). Besides peaks, there are also minima in the electric field intensity, which occur when $Z_{S0} = 0$. The maxima display the cavity resonance, whereas the minima highlight the resonance of the IS ($Z_{S0} = 0$). From Fig. 7(b), an increase in the Q-factor is observed as the resonances of the IS and the cavity are moved closer in the spectrum. Eventually, when the resonances coincide, and in the absence of material losses, the Q-factor is infinite.

C. Cavity with Dispersive and Inhomogenous IS

A model of the IS cavity has been implemented and simulated in COMSOL Multiphysics. The model consists of a cylindrical IS with six Jerusalem crosses placed in free space. Periodic conditions are applied in the z-direction, and the Jerusalem crosses are constructed by conducting surfaces, which are considered to be PECs at first. As the theoretical

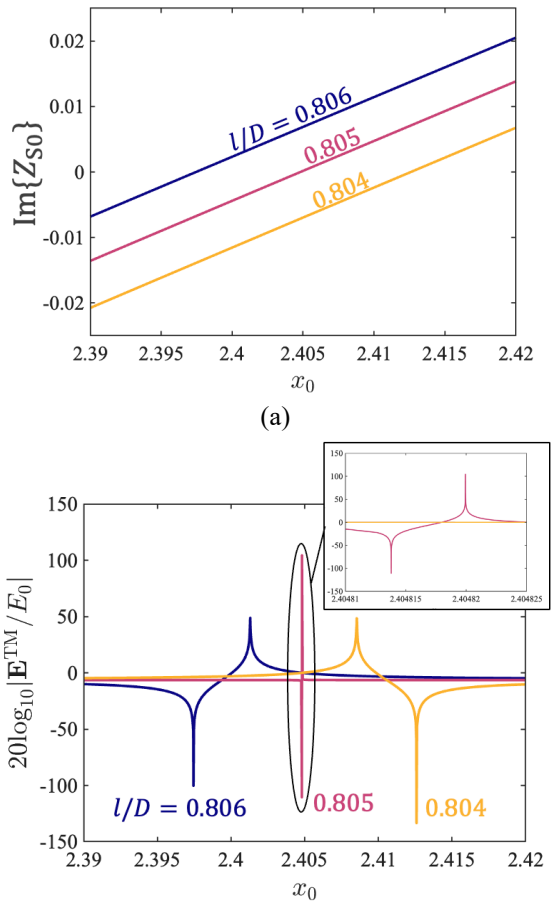

Fig. 7. Analytical results for the empty and lossless IS cavity consisting of an IS of Jerusalem crosses. (a) The imaginary part of the Z_{S0} and (b) the electric field at $(x, y) = (0,0)$ as functions of x_0 for different Jerusalem cross sizes. The parameters for the configuration are $\varepsilon_r = 1$, $D = 2\pi r_c/N$, $N = 6$, $w = 0.0408D$, $d = 0.4D$ and $r_c = 0.383\lambda_{0r}$, where λ_{0r} is the resonance wavelength at the maximum local electric field intensity for the IS cavity with $l/D = 0.805$. An inset is included in (b) to show the spectral details for the case of $l/D = 0.805$.

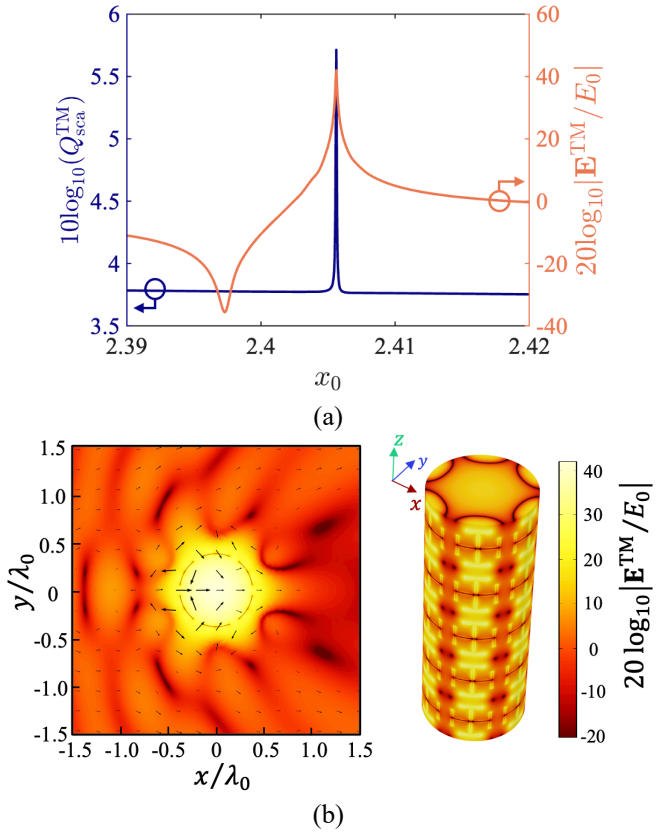

Fig. 8. Simulation results for the empty and lossless IS cavity consisting of six Jerusalem crosses. (a) The scattering efficiency and the electric field at $(x, y) = (0,0)$ as functions of x_0. (b) Electric field (colors) and power flow density (arrows) at the resonance wavelength (λ_{0r}) in the xy-plane (left) and on the surface and inside of the cavity (right). The parameters for the configuration are the same as in Fig. 7 except for l, which has been changed to $l = 0.737D$ for optimal excitation of the cavity resonance.

model of the Jerusalem crosses is an approximation for flat surfaces, the surface needs to be tuned. First, the surface was implemented with the analytically obtained size parameters. Using the eigenfrequency solver, the resonance was found at a much lower frequency ($0.88f_r$ with f_r being the resonance frequency) than predicted by the analytical model. The resonance of the surface was tuned towards the natural resonance of the IS cavity by decreasing l, and the value after optimization is $l/D = 0.737$. The simulation results for the scattering efficiency and the local electric field intensity at $(x, y) = 0$ as functions of x_0 are shown in Fig. 8(a). The local electric field and the power flow density are shown in the Fig. 8(b) at the resonance frequency in an extended region inside and outside of the cylindrical surface impedance. The Q-factor is 30,000 and the local field enhancement is 40 dB. This is considerably lower than that predicted by the analytical results, see Fig. 7(b), and stems from the realized IS not being perfectly smooth, and thus there will be leakage from the IS cavity. The leakage can be minimized by adding more elements to the surface, which decreases the period (D). However, changing D requires adjustment of the other size parameters as well to obtain the required effective surface impedance. Consequently, the size parameter of the Jerusalem crosses can become impractical by having too small D.

Besides the smoothness of the surface impedance, some other factors will also affect the resonance intensity. For example, the Jerusalem cross design considered in this work consists of conductive strips, which will have finite conductivity in practice. Assuming copper strips with the conductivity of $5.8 \cdot 10^7$ S/m, the Q-factor is reduced to around 3,000 for a resonant IS cavity at 1 GHz. Moreover, the maximum field intensity is also reduced by approximately 20 dB compared to the lossless case. A comparison between the analytical and simulation results are presented in Table 1. Additional factors that will affect the performance of the resonator are the truncation of its height as well as account of dielectric losses if a loaded IS cavity is considered. Fabrication imperfections will inevitably affect the performance of the resonator in the form of additional absorption and/or radiation leakage resulting in further reduction of the Q-factor. As in the case of many other highly resonant structures, great care must be taken to the material choice and fabrication.

TABLE I
COMPARISON OF ANALYTIC AND SIMULATION RESULTS FOR THE IS CAVITY CONSISTING OF JERUSALEM CROSSES

Parameter	Analytic Lossless	Simulation Lossless	Simulation Lossy[1]
x_0	2.4048	2.4056	2.4017
l/D	0.805	0.737	0.739
Q-factor	$7\cdot10^{10}$	$3\cdot10^{4}$	$3\cdot10^{3}$
E_{max}/E_0	10^5	10^2	10

[1]Assuming copper conductivity of $5.8\cdot10^7$ S/m and 1 GHz frequency.

V. CONCLUSION

An IS cavity exhibiting quasi-BICs was investigated by analytical and numerical means. The IS cavity consists of a cylindrical IS enabling extreme field localization induced by external waves. This is achieved by utilizing resonant ISs with near-zero effective surface impedances, thus making the cavity partially open. The quasi-BIC is excited by coinciding the resonance of the impedance with the intrinsic cavity modes of the configuration. First, the resonance properties were investigated using an analytical approach. The scattering and local internal fields of different resonant modes were investigated for different polarizations and surface impedances. It is shown that when the IS approaches the PEC limit, the Q-factor diverges to infinity, and the modes become BICs in the limit. Furthermore, a comprehensive examination was performed on the field distribution, Q-factor, and resonance size of the initial three modes, considering their relationship with the surface reactance and resistance, along with the dielectric loading of the cavity. A more realistic design in the form of an IS made of Jerusalem crosses was designed and investigated numerically. The analytical model predicts a Q-factor of ~$7\cdot10^{10}$, whereas the numerical Q-factor is 30,000 due to inhomogeneity of the realistic IS consisting of six elements around the cylindrical curvature. Including material losses (copper), the Q-factor is further reduced to 3,000. Other factors that may affect the performance of the resonator are the truncation of its height as well as dielectric losses if e.g., a printed circuit board substrate is used to realize the IS.

The current study elucidates the fundamental principles underlying cylindrical IS cavities, offering both immediate applicability and guidance for the design of such cavities. The suggested IS cavity design may be of potential interest in the design of filters, antennas, sensors and nonlinear devices. Experimental investigations of the 3-D IS cavity are planned for future work, where the effect of truncation will be studied. Moreover, we will consider configurations of multiple impedance surface layers for the aim of enhancing the scattered field.

REFERENCES

[1] C. W. Hsu, B. Zhen, A. D. Stone, J. D. Joannopoulos, and M. Soljacic, "Bound states in the continuum," *Nat Rev Mater*, vol. 1, no. 9, p. 16048, Sep. 2016, doi: 10.1038/natrevmats.2016.48.

[2] K. Koshelev *et al.*, "Subwavelength dielectric resonators for nonlinear nanophotonics," *Science (1979)*, vol. 367, no. 6475, pp. 288–292, Jan. 2020, doi: 10.1126/SCIENCE.AAZ3985.

[3] A. F. Sadreev, "Interference traps waves in an open system: bound states in the continuum," *Reports on Progress in Physics*, vol. 84, no. 5, p. 055901, Apr. 2021, doi: 10.1088/1361-6633/ABEFB9.

[4] K. Koshelev, G. Favraud, A. Bogdanov, Y. Kivshar, and A. Fratalocchi, "Nonradiating photonics with resonant dielectric nanostructures," *Nanophotonics*, vol. 8, no. 5, pp. 725–745, May 2019, doi: 10.1515/NANOPH-2019-0024.

[5] F. Monticone *et al.*, "Trapping Light in Plain Sight: Embedded Photonic Eigenstates in Zero-Index Metamaterials," *Laser Photon Rev*, vol. 12, no. 5, p. 1700220, May 2018, doi: 10.1002/lpor.201700220.

[6] F. Monticone and A. Alù, "Embedded Photonic Eigenvalues in 3D Nanostructures," *Phys Rev Lett*, vol. 112, no. 21, p. 213903, May 2014, doi: 10.1103/PhysRevLett.112.213903.

[7] R. E. Jacobsen, A. Krasnok, S. Arslanagic, A. V. Lavrinenko, and A. Alu, "Boundary-Induced Embedded Eigenstate in a Single Resonator for Advanced Sensing," *ACS Photonics*, vol. 9, no. 6, pp. 1936–1943, Jun. 2022, doi: 10.1021/ACSPHOTONICS.1C01840.

[8] M. V. Rybin *et al.*, "High-Q Supercavity Modes in Subwavelength Dielectric Resonators," *Phys Rev Lett*, vol. 119, no. 24, p. 243901, Dec. 2017, doi: 10.1103/PhysRevLett.119.243901.

[9] M. Odit, K. Koshelev, S. Gladyshev, K. Ladutenko, Y. Kivshar, and A. Bogdanov, "Observation of Supercavity Modes in Subwavelength Dielectric Resonators," *Advanced Materials*, vol. 33, no. 1, p. 2003804, Jan. 2021, doi: 10.1002/ADMA.202003804.

[10] R. E. Jacobsen and S. Arslanagić, "Supercavity mode in a single metallic resonator," *Appl Phys Lett*, vol. 123, no. 22, p. 221701, Nov. 2023, doi: 10.1063/5.0174480/2924897.

[11] F. S. Cuesta *et al.*, "Nonscattering Metasurface-Bound Cavities for Field Localization, Enhancement, and Suppression," *IEEE Trans Antennas Propag*, vol. 68, no. 3, pp. 1689–1703, Mar. 2020, doi: 10.1109/TAP.2019.2938661.

[12] A. Toscano, A. Monti, and F. Bilotti, "Optical cloaking of cylindrical objects by using covers made of core–shell nanoparticles," *Optics Letters, Vol. 36, Issue 23, pp. 4479-4481*, vol. 36, no. 23, pp. 4479–4481, Dec. 2011, doi: 10.1364/OL.36.004479.

[13] A. Toscano, A. Monti, F. Bilotti, S. H. Raad, and Z. Atlasbaf, "Maximizing the forward scattering of dielectric nanoantennas through surface impedance coatings," *Optics Letters, Vol. 47, Issue 10, pp. 2386-2389*, vol. 47, no. 10, pp. 2386–2389, May 2022, doi: 10.1364/OL.456958.

[14] R. E. Jacobsen, A. V. Lavrinenko, and S. Arslanagic, "Scattering Properties of High-Permittivity Dielectric Resonators Embedded with Impedance Sheets," *2022 3rd URSI Atlantic and Asia Pacific Radio Science Meeting (AT-AP-RASC)*, pp. 1–4, May 2022, doi: 10.23919/AT-AP-RASC54737.2022.9814262.

[15] Y. R. Padooru, A. B. Yakovlev, P. Y. Chen, and A. Alù, "Analytical modeling of conformal mantle cloaks for cylindrical objects using sub-wavelength printed and slotted arrays," *J Appl Phys*, vol. 112, no. 3, p. 034907, Aug. 2012, doi: 10.1063/1.4745888.

[16] C. Qian *et al.*, "Experimental Observation of Superscattering," *Phys Rev Lett*, vol. 122, no. 6, p. 063901, Feb. 2019, doi: 10.1103/PHYSREVLETT.122.063901.

[17] V. I. Shcherbinin, V. I. Fesenko, T. I. Tkachova, and V. R. Tuz, "Superscattering from Subwavelength Corrugated Cylinders," *Phys Rev Appl*, vol. 13, no. 2, p. 024081, Feb. 2020, doi: 10.1103/PHYSREVAPPLIED.13.024081.

[18] Z. Ruan and S. Fan, "Superscattering of light from subwavelength nanostructures," *Phys Rev Lett*, vol. 105, no. 1, p. 013901, Jun. 2010, doi: 10.1103/PHYSREVLETT.105.013901.

[19] R. E. Jacobsen, A. V. Lavrinenko, and S. Arslanagić, "Reconfigurable dielectric resonators with imbedded impedance surfaces - From enhanced and directional to suppressed scattering," *Appl Phys Lett*, vol. 122, no. 8, p. 81701, Feb. 2023, doi: 10.1063/5.0139695/2872894.

[20] G. Loukos, J. C. Vardaxoglou, G. Loukos, and J. C. Vardaxoglou, "Propagation inside strip grating FSS waveguides with cylindrical cross-

section," *Electron Lett*, vol. 31, no. 10, pp. 778–779, May 1995, doi: 10.1049/EL:19950565.

[21] A. Uzer and T. Ege, "Scattering from periodically spaced longitudinal slots on a conducting cylinder," *Electrical Engineering 2004 87:6*, vol. 87, no. 6, pp. 291–293, Sep. 2004, doi: 10.1007/S00202-004-0256-0.

[22] Constantine A. Balanis, *Advanced Engineering Electromagnetics*, 2nd ed. John Wiley & Sons, 1989.

[23] C. F. Bohren and D. R. Huffman, *Absorption and scattering of light by small particles*, 1st ed. New York: John Wiley & Sons: Hoboken, 1983.

[24] A. Sihvola, D. C. Tzarouchis, P. Ylä-Oijala, H. Wallén, and B. Kong, "Resonances in small scatterers with impedance boundary," *Phys Rev B*, vol. 98, no. 23, p. 235417, Dec. 2018, doi: 10.1103/PHYSREVB.98.235417.

[25] O. Luukkonen *et al.*, "Simple and accurate analytical model of planar grids and high-impedance surfaces comprising metal strips or patches," *IEEE Trans Antennas Propag*, vol. 56, no. 6, pp. 1624–1632, Jun. 2008, doi: 10.1109/TAP.2008.923327.

[26] C. R. Simovski, P. de Maagt, and I. V. Melchakova, "High-impedance surfaces having stable resonance with respect to polarization and incidence angle," *IEEE Trans Antennas Propag*, vol. 53, no. 3, pp. 908–914, Mar. 2005, doi: 10.1109/TAP.2004.842598.

[27] T. Christensen, A. P. Jauho, M. Wubs, and N. A. Mortensen, "Localized plasmons in graphene-coated nanospheres," *Phys Rev B Condens Matter Mater Phys*, vol. 91, no. 12, p. 125414, Mar. 2015, doi: 10.1103/PHYSREVB.91.125414.

[28] A. Monti, J. C. Soric, A. Alù, A. Toscano, and F. Bilotti, "Anisotropic Mantle Cloaks for TM and TE Scattering Reduction," *IEEE Trans Antennas Propag*, vol. 63, no. 4, pp. 1775–1788, Apr. 2015, doi: 10.1109/TAP.2015.2396532.

Rasmus E. Jacobsen received the B.Sc. and M.Sc. degrees in Electrical Engineering from the Department of Electrical Engineering, Technical University of Denmark (DTU), in 2015 and 2017, respectively. He obtained his Ph.D. degree from Department of Photonics Engineering, DTU, in 2021. Since 2021 he has been a Postdoctoral researcher at the Division of Electromagnetic Systems, Department of Space research and technologies, DTU. Rasmus E. Jacobsen was a Visiting Scholar at the Advanced Science Research Center, the City University of New York City (CUNY), USA, in 2020 and at the Faculty of Physics, ITMO University, St. Petersburg, Russia, in 2019. His current research interests include electromagnetic wave-matter interaction, functional material structures, scattering analysis and measurements, and electrically small antennas. He was recipient of the Young Scientist award at the URSI Altantic Radio Science Meeting (AT-AP- RASC) 2022.

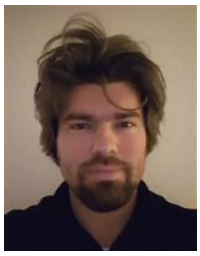

Samel Arslanagić was born in Sarajevo, Bosnia and Herzegovina, on July 28, 1979. He obtained his M.Sc. and Ph.D. degrees from the Technical University of Denmark (DTU) in 2004 and 2007, respectively. Since 2009 he has been on the faculty of the Department of Electrical Engineering as Assistant Professor (2009-2012) and Associate Professor (2012-2022). Since 2021 he has been on the faculty of Department for Space Research and Technology, where he is Head of the Division for Electromagnetic Systems which also hosts and operates the DTU Electromagnetic Test Centre. Samel Arslanagić was a Visiting Scholar at Electromagnetics Laboratory, University of Arizona, USA, in the fall of 2005 and summer of 2011. His research interest is in the area of applied electromagnetics, spanning wave-matter interaction and scattering, functional material structures from, RCS measurements and the broad area of electromagnetic education. He is the author or co-author of more than 40 journal papers, 80 conference papers, and 4 book chapters. He received the 2018 DTU Student Union's "Lecturer of the Year" award for his teaching in electromagnetics and wireless communications. In recognition of his excellent research and dissemination of natural sciences to a broader audience, he was awarded the 2021 H.C. Ørsted Medal in Silver by The Society for Dissemination of Natural Sciences established by H.C. Ørsted in 1824.